

DISTRIBUTED PRECONDITIONING FOR THE PARAMETRIC HELMHOLTZ EQUATION

WOUTER GERRIT VAN HARTEN* AND LAURA SCARABOSIO*

Abstract. In this work, we address the efficient computation of parameterized systems of linear equations, with possible nonlinear parameter dependence. When the matrix is highly sensitive to the parameters, mean-based preconditioning might not be enough. For this scenario, we explore an approach in which several preconditioners are placed in the parameter space during a precomputation step. To determine the optimal placement of a limited number of preconditioners, we estimate the expected number of iterations with respect to a given preconditioner a priori and use a location-allocation strategy to optimize the placement of the preconditioners. We elaborate on our methodology for the Helmholtz problem with exterior Dirichlet scattering at high frequencies, and we estimate the expected number of GMRES iterations via a gray-box Gaussian process regression approach. We illustrate our approach in two practical applications: scattering in a domain with a parametric refractive index and scattering from a scatterer with parameterized shape. Using these numerical examples, we show how our methods leads to runtime savings of about an order of magnitude. Moreover, we investigate the effect of the parameter dimension and the importance of dimension anisotropy on their efficacy.

Key words. Preconditioning, Uncertainty quantification, Gray-box Gaussian process regression, Helmholtz equation

MSC codes. 35B30, 35J05, 60G15, 65F08, 65N22

1. Introduction. In many scientific and engineering applications, solving large systems of parameterized linear equations is a fundamental task. These systems appear in, among others, uncertainty quantification, PDE-constrained optimization, and inverse problems, where the repeated solution of linear systems is a major computational bottleneck.

For a given linear system, i.e. a fixed parameter value, various methods for its efficient solution exist. While direct methods are feasible for systems of moderate size, larger systems require iterative solvers like Krylov methods [40]. Their performance is highly dependent on the system's condition number, which can be reduced by using a preconditioner [67]. Performing preconditioning requires itself some computational resources, which are compensated by the realized reduction in Krylov iterations. Choosing the right preconditioner is application-specific and extensively studied [51, 67].

When solving multiple linear systems, we would like to reduce the computational load. One could, for example, try to parameterize the preconditioner [19]. Another well-studied option is to recycle either the Krylov subspaces [50] or the preconditioner(s). For the Helmholtz application we will consider, Krylov subspace recycling has been considered in [41]. In this work, we will focus our attention on preconditioner recycling.

For this, we could take inspiration from [34], and apply a single preconditioner to multiple systems. Initial exploration of this approach has been performed for stochastic spectral finite element methods applied to the diffusion equation [31, 44, 52] and the Helmholtz equation [66, 41]. Preconditioning was performed through block-diagonal

*IMAPP, Radboud University, The Netherlands (w.vanharten@science.ru.nl)

preconditioning, where a single mean-based preconditioner is used in a block-diagonal setting. These ideas were then applied to the much more challenging Navier-Stokes equations, where the stochastic Galerkin discretization of said equations was investigated numerically [54]. Outside the stochastic Galerkin framework, we can make use of mean-based preconditioning as well, which was initially explored for the diffusion equation [26, 29]. To get a complete overview of the history of mean-based preconditioning, we refer the reader to an excellent overview by Owen Pembrey [53, Section 4.7]. While mean-based preconditioning is computationally efficient, it might break down if the effect of parameter changes on the matrix is large.

Improvements could be gained by considering multiple preconditioners throughout the parameter space. This has been investigated in [65] for the diffusion equation with short correlation lengths, focused on Voronoi quantizers placed without prior knowledge of the parameter locations. For the Helmholtz equation, a greedy approach for known parameter locations was presented in [53, Section 4.6]. However, this approach requires prior knowledge about the maximum iterations and the distance function on the parameter space, and it might struggle if the problem has hidden parameter anisotropy or a high dimension.

Our approach exploits the structure and a-priori knowledge of parameter locations and overcomes the limitations in [53]. The main novelty of our work is to train a surrogate model to predict the number of Krylov iterations needed and determine preconditioner placement while incorporating dimension anisotropy. Since computing the best locations to place the preconditioners is known to be NP-hard [59], we use a location-allocation heuristic [9]. After having introduced the problem in Section 2, Section 3 explains this process and Section 4 discusses methods to obtain such a surrogate using known convergence bounds of the Krylov method.

To validate our approach, we apply it to high-frequency Helmholtz scattering with heterogeneous coefficients which have C^1 -parameter dependence, which is addressed in Section 5. The Helmholtz equation is known to be particularly ill-conditioned at high frequencies, making it a great benchmark for evaluating preconditioning strategies [12, 34]. For the Helmholtz equation, [34] derived frequency-explicit upper bounds on the number of GMRES iterations for a given tolerance. We exploit this a priori knowledge to build a good prior mean and kernel of our surrogate, a gray box Gaussian process regression model [55]. The Gaussian process is trained with an active learning strategy using the parameter values for which the linear system needs to be solved anyway. Choosing the right training point is no simple task either, as evaluating the training points can be very expensive. Since in particular the costs of evaluating a training point is not constant, we use a cost-aware optimization strategy to train our surrogate model. We consider both an affine parameter dependence and a setting with a parameterized domain, going beyond the affine case.

Section 6 presents numerical studies, analyzing isotropic and anisotropic parameter dependencies. Finally, we end with a summary and concluding remarks in Section 7.

2. Problem statement. Let $\{\mathbb{A}(\mathbf{y}_i)\}_{\mathbf{y}_i \in W}$ be a family of parameterized matrices with parameter vectors $W = \{\mathbf{y}_i \in Y\}_{i \in I}$ for some finite index set I and $Y = \prod_{i=1}^N Y_i$ with Y_i a bounded interval in \mathbb{R} . Our goal is to solve the system $\mathbb{A}(\mathbf{y}_i)\mathbf{u}(\mathbf{y}_i) = b$ for all parameter vectors \mathbf{y}_i . We turn our attention to preconditioned Krylov methods and consider the preconditioned system to find the high-dimensional

vector $\mathbf{u}(\mathbf{y}_i)$ for $\mathbf{y}_i \in W$:

$$(2.1) \quad \mathbb{P}(\mathbf{y}_i)\mathbb{A}(\mathbf{y}_i)\mathbf{u}(\mathbf{y}_i) = \mathbb{P}(\mathbf{y}_i)b.$$

We do not specify the exact choice of preconditioner for now, but we will be more explicit in Section 4. We place N_{pc} preconditioners $\mathbb{P}(\hat{\mathbf{y}}_k) \in Y$. These preconditioners form a partition W_k of W , each with a selected preconditioner location $\hat{\mathbf{y}}_k$. Then, we set $\mathbb{P}(\mathbf{y}_i) = \mathbb{P}(\hat{\mathbf{y}}_k)$ for $\mathbf{y}_i \in W$.

We note that the parameter space Y may be isotropic or anisotropic, implying that the effect of different parameter dimensions on the conditioning of the system may not be equal. Moreover, we will consider left preconditioning. Right- and split methods can be treated similarly.

To find a good preconditioning strategy, we will place several preconditioners in the parameter space in the next section.

3. Preconditioner placement. To place the preconditioners in Y , we rely on a problem-specific approximation of the expected number of iterations, which we denote by \tilde{m} :

$$\tilde{m}(\mathbf{y}, \hat{\mathbf{y}}) := \# \text{ Krylov iterations to solve } \mathbb{P}(\hat{\mathbf{y}})\mathbb{A}(\mathbf{y})x = \mathbb{P}(\hat{\mathbf{y}}), \text{ for } \mathbf{y}, \hat{\mathbf{y}} \in Y,$$

and by

$$(3.1) \quad N_{ratio} = \frac{\tau_{pc}}{\tau_{Krylov}}$$

the ratio between the computation time of a preconditioner τ_{pc} and τ_{Krylov} , the time to perform a single Krylov iteration. Moreover, we assume that the number of Krylov iterations required is invariant under translations:

ASSUMPTION 3.1. *We have $\tilde{m}(\mathbf{y}, \hat{\mathbf{y}}) = \tilde{m}(\mathbf{y} + \tilde{\mathbf{y}}, \hat{\mathbf{y}} + \tilde{\mathbf{y}})$, for all $\mathbf{y}, \tilde{\mathbf{y}}$, and $\hat{\mathbf{y}}$ in Y .*

This way, it is sufficient to define $m(\cdot)$ such that, for $\mathbf{y}, \hat{\mathbf{y}} \in Y$,

$$m(\mathbf{y} - \hat{\mathbf{y}}) := \tilde{m}(\mathbf{y}, \hat{\mathbf{y}}).$$

Although Assumption 3.1 is not always satisfied, it provides an effective framework for building a good surrogate of $m(\cdot)$ that is efficient to evaluate. When not fulfilled, we can think of our surrogate as incorporating a modeling approximation.

We must determine N_{pc} , the number of preconditioners first. A small N_{pc} wastes computational potential, while a larger N_{pc} increases the cost of the preconditioning strategy. For now, we fix N_{pc} and discuss its choice in Section 3.3. For the time being, we assume we have $m(\cdot)$ and discuss its construction in Section 4.

To place the preconditioners efficiently, we need to solve

$$(3.2) \quad \min_{\{\hat{\mathbf{y}}_k\}_{k=1}^{N_{pc}}} \sum_{\mathbf{y}_j} m\left(\mathbf{y}_j - \hat{\mathbf{y}}\left(\mathbf{y}_j \mid \{\hat{\mathbf{y}}_k\}_{k=1}^{N_{pc}}\right)\right),$$

where

$$\hat{\mathbf{y}}\left(\mathbf{y}_j \mid \{\hat{\mathbf{y}}_k\}_{k=1}^{N_{pc}}\right) = \arg \min_{\hat{\mathbf{y}} \in \{\hat{\mathbf{y}}_k\}_{k=1}^{N_{pc}}} m(\mathbf{y}_j - \hat{\mathbf{y}})$$

maps each parameter location \mathbf{y}_i to its assigned preconditioner location $\hat{\mathbf{y}}_k$. Equation (3.2) is equivalent to the NP-hard *uncapacitated facility location problem* [9, 59]. Therefore, we resort to iterative algorithms for computational feasibility, despite the possible occurrence of local minima [16].

We turn our attention to the well-known *location-allocation* algorithm [20, 45], which iterates through a location and an allocation step. First, the preconditioners are initialized (Section 3.1). Then the values in W are clustered iteratively, where each step assigns parameters to the preconditioner with the lowest expected number of Krylov iterations. The preconditioner location is then optimized to minimize Krylov iterations given the assigned parameter values, and this process continues until convergence or diminishing returns (Section 3.2).

3.1. Initialization. Since the optimization problem (3.2) has many local minima, good initialization is key. Several initialization methods have been considered; random initialization proved inefficient, Quasi Monte Carlo sequences can incorporate anisotropy [39] but require many optimization steps, and Bayesian optimization is effective but suffers from the curse of dimensionality. We use greedy initialization instead, which is effective and computationally inexpensive. This means iteratively placing preconditioners at the parameter location with the highest expected number of Krylov iterations.

3.2. Location-allocation. After initialization, we iterate through location and allocation steps. In each location step, we need to find the center of each cell in the partition W_k . This boils down to computing, for every element of the partition:

$$(3.3) \quad \arg \min_{\hat{\mathbf{y}}_* \in Y} \sum_{\mathbf{y}_j \in W_k} m(\mathbf{y}_j - \hat{\mathbf{y}}_*).$$

This minimization problem, also known as the *Weber problem* or the *generalized Fermat problem*, is very challenging to solve [9, 43]. The Weiszfeld algorithm solves this efficiently for Euclidean distances [21, 68] and the applicability of generalized versions [25, 22] depend on the structure of $m(\cdot)$. We thus resort to an iterative approach to solve (3.3) by employing a general-purpose optimizer readily available in many programming languages. For large values of N_{pc} , the location step is costly. However, greedy initialization tends to initialize near local minima in these cases.

In the allocation step, each $\mathbf{y}_i \in W$ is assigned to the preconditioner minimizing Krylov iterations, and we obtain a partition new W_k of W . This defines a *generalized Voronoi diagram* [15].

REMARK 3.2. *Differently from previous work [34], we do not assume $\{\hat{\mathbf{y}}_k\}_{k=1}^{N_{pc}} \subset W$. Restricting the preconditioners to the parameter locations may be suboptimal and allowing the preconditioners at any point in the parameter enables continuous optimization.*

3.3. Determining the number of preconditioners. Determining N_{pc} resembles a clustering problem. Instead, we re-use the greedy initialization: at each step, we estimate the total computation time

$$\tau_{est}(N_{pc}) = N_{ratio}N_{pc} + \sum_{\mathbf{y}_j} m(\mathbf{y}_j - \hat{\mathbf{y}}(\mathbf{y}_j)),$$

and, if $\tau_{est}(N_{pc}) > \tau_{est}(N_{pc} - 1) > \tau_{est}(N_{pc} - 2)$, we discard the last two placed preconditioners and set $N_{pc} = N_{pc} - 2$. Although this procedure has no rigorous guarantee to find the optimal value for N_{pc} , it gave us satisfactory results at a cheap cost. We note that other alternatives are available [63, 56, 64], but these require multiple expensive clustering runs.

We summarize the preconditioner placement in Algorithm 3.1.

Algorithm 3.1 Preconditioner placement

Input $W, N_{ratio}, pc_{fixed} = \{\}$

▷ Parameter locations, Cost ratio, Precomputed preconditioner locations

Output pc_{loc}

▷ Computed preconditioner locations

1: $N_{pc} \leftarrow |pc_{fixed}| - 1$

▷ The number of preconditioners

2: $pc_{loc} \leftarrow pc_{fixed}$

▷ Preconditioner locations

3: $cost \leftarrow \left\{ \infty, N_{ratio} * N_{pc} + \sum_{\mathbf{y}_i \in W} m(\mathbf{y}_i, \hat{\mathbf{y}}(\mathbf{y}_i | pc_{fixed})) \right\}$

▷ Expected costs of the preconditioning strategy

4: **while** $cost$ not increasing twice in a row **do** ▷ **Initialization** and compute N_{pc}

5: $N_{pc} \leftarrow N_{pc} + 1$

6: $pc_{loc} \leftarrow pc_{loc} \cup \{\arg \max_{\mathbf{y}_i \in W} m(\mathbf{y}_i, \hat{\mathbf{y}}(\mathbf{y}_i | pc_{loc}))\}$

7: $cost \leftarrow cost \cup \{N_{ratio} * N_{pc} + \sum_{\mathbf{y}_i \in W} m(\mathbf{y}_i, \hat{\mathbf{y}}(\mathbf{y}_i | pc_{loc}))\}$

8: **end while**

9: $N_{pc} \leftarrow N_{pc} - 2, pc_{loc} \leftarrow pc_{loc}[: -2]$

▷ Discard last two preconditioners

10: **while** Preconditioner has changed **and** compute time < strategy gain **do**

▷ continue **location-allocation** as long as there is change and it is worthy

11: $W_k \leftarrow partition(W, pc_{loc}, m)$

▷ Compute the partitions W_k

12: **for** $\hat{\mathbf{y}}_k \in pc_{loc}$ **do**

▷ Location step

13: $\hat{\mathbf{y}}_k \leftarrow \arg \min_{\mathbf{y} \in Y} \sum_{\mathbf{y}_i \in W_k[\hat{\mathbf{y}}_k]} m(\mathbf{y}_i - \hat{\mathbf{y}}')$

14: **end for**

15: **end while**

16: **return** pc_{loc}

REMARK 3.3 (Concentration of measure for isotropic parameter space). *As the parameter dimension grows, the distance to the origin, and hence the number of Krylov iterations, concentrates [1]. Thus, in high-dimensional isotropic parameter space, the expected number of Krylov iterations with a mean-based preconditioner is nearly uniform. If this number is below the cost ratio, mean-based preconditioning is optimal; otherwise, separate preconditioners per parameter value are preferred. Consequently, in this case the optimal value of N_{pc} is either one if $m(\mathbb{E}[\|X\|_2]) < N_{ratio}$, or the cardinality of W .*

4. Estimating $m(\cdot)$ for GMRES. To apply Algorithm 3.1, we need a function approximating the number of Krylov iterations. We propose an approach based on Gaussian process regression (GPR), using a priori bounds on the number of iterations to initialize a gray-box GPR [3]. We illustrate this on GMRES iterations with LU preconditioning, setting $\mathbb{P}(\mathbf{y}_i) = \mathbb{A}(\hat{\mathbf{y}}(\mathbf{y}_i))^{-1}$ to solve

$$(4.1) \quad \mathbb{A}(\hat{\mathbf{y}}(\mathbf{y}_i))^{-1} \mathbb{A}(\mathbf{y}_i) \mathbf{u}(\mathbf{y}_i) = \mathbb{A}(\hat{\mathbf{y}}(\mathbf{y}_i))^{-1} \mathbf{b}, \quad \text{for } \mathbf{y}_i \in W$$

Next, we construct the gray-box GPR in Sections 4.1–4.3 and the training of the GPR is presented in Section 4.4. This surrogate can then be used in the preconditioner placement strategy outlined in Section 3.

4.1. Gray-box GPR. To infer $m(\cdot)$, we use an active learning strategy based on Gaussian process regression and an acquisition function that balances knowledge gain and training cost. The uncertainty band provided by the Gaussian process, and the GPR will allow us to define a termination criterion. We consider a Gray-box GPR [3], modelling m as a nonlinear function of a Gaussian process, with which we include prior knowledge in our estimate.

For GMRES, we use the Elman estimate [27, 34], which states that the relative tolerance ε at the m -th GMRES iteration is bounded by

$$(4.2) \quad \varepsilon = \frac{\|r_m\|}{\|r_0\|} \leq \left(\frac{2\sqrt{\alpha}}{\alpha + 1} \right)^m,$$

with $\|I - \mathbb{A}^{-1}(\hat{\mathbf{y}}(\mathbf{y}_i))\mathbb{A}(\mathbf{y}_i)\| \leq \alpha < 1$, if we are solving equation (4.1). Therefore, an upper bound on $\|I - \mathbb{A}^{-1}(\hat{\mathbf{y}}(\mathbf{y}_i))\mathbb{A}(\mathbf{y}_i)\|$ provides us with an upper bound on the required GMRES iterations. Moreover, if we estimate α as a function of $\mathbf{y}_i - \hat{\mathbf{y}}(\mathbf{y}_i)$, equation (4.2) provides us with an estimate for $m(\mathbf{y}_i - \hat{\mathbf{y}}(\mathbf{y}_i))$. Hence, we rewrite (4.2) and define

$$(4.3) \quad m(\mathbf{y}) := \ln(\varepsilon) \ln \left(\frac{2\sqrt{\mathbb{E}[\alpha(\mathbf{y})]}}{\mathbb{E}[\alpha(\mathbf{y})] + 1} \right)^{-1},$$

for $\mathbf{y} \in Y$ and where, exploiting translation invariance, $\alpha(\mathbf{y})$ models α in terms of \mathbf{y} , sampled from a Gaussian process

$$(4.4) \quad \alpha(\mathbf{y}) \sim GP(\mu_0(\mathbf{y}, C), K(\mathbf{y}, \mathbf{y}')),$$

with prior mean $\mu_0(\mathbf{y}, C)$ possibly dependent on N_{hyp} hyperparameters $C = (C_1, \dots, C_{N_{hyp}}) \in \mathbb{R}^{N_{hyp}}$, and kernel $K(\mathbf{y}, \mathbf{y}')$. The prior mean is problem-specific, and needs to be chosen carefully. In Section 5, we will expand on this in the case of Helmholtz scattering. Moreover, we elaborate on the kernel choice in Section 4.2. To simplify the notation, we set

$$(4.5) \quad g(\alpha) := \ln(\varepsilon) \ln \left(\frac{2\sqrt{\alpha}}{\alpha + 1} \right)^{-1}, \quad \text{such that} \quad m(\mathbf{y}) = g(\mathbb{E}[\alpha(\mathbf{y})]).$$

REMARK 4.1 (Nonlinearity of $g(\alpha)$). *Ideally, we would like to use $m(\mathbf{y}) = \mathbb{E}[g(\alpha(\mathbf{y}))]$, as this accurately describes the expected value. However, this requires integrating over the probability space, which is analytically intractable and computationally expensive.*

To perform the preconditioner placement outlined in Section 3 accurately, it is important for $m(\cdot)$ to be accurate near the boundaries of the partition $\{W_k\}_k$: this determines the distance between the preconditioners, and therefore, N_{pc} . At the boundaries of the partitions, the values of α are neither very low or high. As we can see in Fig. 1, $g(\alpha)$ is concave for small ($\alpha < 0.01$) values of α , and convex for large. Outside of these regions, that is in the area $[0.01, 0.03]$ in Fig. 1, $g(\alpha)$ remains rather linear, such that the effect of switching $\mathbb{E}[\cdot]$ and $g(\cdot)$ is minimal.

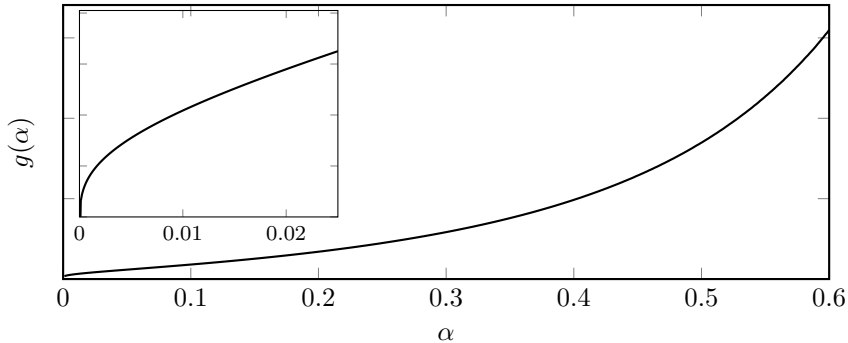


Fig. 1: Plot of $g(\alpha)$ up to a constant from 0 to 0.6.

REMARK 4.2 (Different estimates). *The Elman estimate is based on the field of values of $\mathbb{A}(\hat{\mathbf{y}}(\mathbf{y}_i))^{-1}\mathbb{A}(\mathbf{y}_i)$, but different estimates could be considered, based on eigenvalues or pseudospectra, see [28] for a clear overview. However, different estimates all have their strengths and weaknesses, and we considered the Elman estimate because of the available bounds for the field of values for the Helmholtz equation.*

4.2. Kernel. For our method to work efficiently in high parameter dimensions, we have to be careful in choosing the kernel. The *curse of dimensionality* poses a challenge in Gaussian processes. Kernel selection may seem like an art, and [23, Chapter 2] provides a useful guide in the ‘Kernel cookbook’, while an overview of dimensionality issues can be found in [6]. For computational efficiency, we consider univariate kernels [24, 48]:

$$(4.6) \quad K(\mathbf{y}, \mathbf{y}') = \sum_{i=1}^N K_i(y_i, y'_i).$$

Each kernel $K_i(\cdot, \cdot)$ combines a symmetric Matérn kernel [23] and a linear kernel, ensuring zero variance at the origin and increasing variance as $\|\mathbf{y}\| \rightarrow \infty$:

$$\begin{aligned} K_i(y_i, y'_i) &= K_i^{\text{sym}}(K_{\text{lin}}(y_i, y'_i)K_{\nu}^{\text{Matérn}}(y_i, y'_i)) \\ &= \sum_{(m_1, m_2) \in \{-1, 1\}^2} K_{\text{lin}}(m_1 y_i, m_2 y'_i) K_{\nu}^{\text{Matérn}}(m_1 y_i, m_2 y'_i), \end{aligned}$$

where $K_{\nu}^{\text{Matérn}}(\cdot, \cdot)$ is the standard Matérn kernel and $K_{\text{lin}}(\cdot, \cdot)$ is a linear kernel [23]. The symmetrization has been performed using the *sum over orbits* technique [23] and for minimal regularity, we choose $\nu = \frac{1}{2}$ for the smoothness parameter. We take the correlation lengths of the Matérn kernels to be inversely proportional to the importance of the corresponding parameter dimension, to reduce the model complexity. In Section 5, we outline how we can obtain these anisotropy weights.

4.3. Hyperparameter tuning. In the previous sections, we have introduced hyperparameters in the prior mean. The standard approach of selecting them is by maximizing the likelihood of the training data [42, 55] given the prior mean and kernel. However, since we use correlation lengths inversely proportional to the importance of the dimension to reduce computational cost, large correlation lengths negatively affect the accuracy of the chosen hyperparameters.

To address this, we choose hyperparameters minimizing the mean squared error of the training data with respect to the prior mean:

$$C = (C_1, \dots, C_{N_{hyp}}) = \arg \min_{C^* \in \mathbb{R}^{N_{hyp}}} \sum_{\mathbf{y}_{i,train}} (\mu_0(\mathbf{y}_{i,train} | C^*) - \alpha_{\mathbf{y}_{i,train}})^2,$$

where $\mathbf{y}_{i,train}$ are the training locations and $\alpha_{\mathbf{y}_{i,train}}$ the corresponding values for α . We solve this minimization problem using a gradient-based optimization routine, as the objective function is smooth and has explicit derivatives.

4.4. Training the Gray-box GPR. In our active learning strategy, we initialize a mean-based preconditioner at $\bar{\mathbf{y}}$, the center of W , and solve the linear system (5.2) using the mean-based preconditioner $\mathbb{A}(\bar{\mathbf{y}})^{-1}$ for training points $\mathbf{y}_{i,train} \in W$, recording $\{\mathbf{y}_{i,train}, \alpha(\mathbf{y}_{i,train})\}$. These evaluations provide both linear system solutions and training pairs. Following [3], we iteratively select training points from W by maximizing an acquisition function $f_{acq} : W \rightarrow \mathbb{R}$.

Since evaluation costs depend on $m(\mathbf{y})$, we account for this in f_{acq} , similarly to cost-aware Bayesian optimization [47, 69]. We define f_{acq} as the variance-to-cost ratio, capped at a cutoff-value $m_{\max} = \frac{\tau_{pc}}{\tau_{GMRES}}$, ensuring unimportant training data is not selected. The values of τ_{pc} can be calculated when computing the mean-based preconditioner and τ_{GMRES} can be computed on the fly using the computed training points. This is a particular instance of the well-studied expected improvement per unit cost [61]:

$$(4.7) \quad f_{acq}(\mathbf{y}; m_{\max}) := \begin{cases} \frac{\mathbb{V}[g(\alpha(\mathbf{y}))]}{\mathbb{E}[g(\alpha(\mathbf{y}))]} & \text{for } \mathbb{E}[g(\alpha(\mathbf{y}))] \leq m_{\max}, \\ -\infty & \text{else,} \end{cases}$$

where $\mathbb{E}[g(\alpha(\mathbf{y}))]$ and $\mathbb{V}[g(\alpha(\mathbf{y}))]$ are the mean and variance of $g(\alpha(\mathbf{y}))$ from (4.5), respectively. To compute (4.7), we approximate $\mathbb{V}[m(\mathbf{y})]$ by central differences:

$$\mathbb{V}[g(\alpha(\mathbf{y}))] \approx \frac{g(\mathbb{E}[\alpha(\mathbf{y})] + \mathbb{V}[\alpha(\mathbf{y})]) - g(\mathbb{E}[\alpha(\mathbf{y})] - \mathbb{V}[\alpha(\mathbf{y})])}{2}.$$

This will introduce a small bias but enables for efficient computations as the expected values can be computed directly [7, Chapter 6].

Each new training point is then selected by

$$\mathbf{y}_{i,train} = \arg \max_{\mathbf{y}_i \in W} f_{acq}(\mathbf{y}_i - \bar{\mathbf{y}}; m_{\max}),$$

and each time we add a training point, we fit the hyperparameters again. The acquisition function requires the hyperparameters itself and hence, to start the training, we initialize the Gaussian process with two points, $\bar{\mathbf{y}}$ and $\mathbf{y}_{\min} = \arg \min_{\mathbf{y} \in W} \mu_0(\mathbf{y}, 1)$. At $\bar{\mathbf{y}}$, we set $\alpha(\mathbf{0}) = g^{-1}(1)$, and at \mathbf{y}_{\min} we solve $\mathbb{A}(\bar{\mathbf{y}})^{-1} \mathbb{A}(\mathbf{y}_{\min}) = \mathbb{A}(\bar{\mathbf{y}})^{-1} b$ to obtain $m(\mathbf{y}_{\min} - \bar{\mathbf{y}})$.

Training continues until the surrogate model reaches a satisfactory accuracy. Ideally, accuracy is assessed using a test set, but this is computationally expensive. Instead, we use the *Stabilizing predictions* (SP) stopping criterion [8, 18], stopping training when the averaged disagree ratio drops below 1%. Since this criterion is originally defined on labelled data, we adapt it to the continuous scale of $m(\cdot)$ by defining an ‘agree’ whenever the relative difference between two iterations is lower than 1%, with a minimum of 1 iteration.

4.5. Assembling the surrogate. With the collected training points $W_{train} = \{\mathbf{y}_{1,train}, \dots, \mathbf{y}_{N_{train},train}\}$ and obtained Gaussian process values $\boldsymbol{\alpha}_{train} = \{\alpha_{\mathbf{y}_{1,train}}, \dots, \alpha_{\mathbf{y}_{N_{train},train}}\}$, we define $m(\cdot)$ as (4.3), with

$$\mathbb{E}[\alpha(\mathbf{y})] = \mu_0(\mathbf{y}) + K(\mathbf{y} + \bar{\mathbf{y}}, W_{train})^\top K(W_{train}, W_{train})^{-1}(\boldsymbol{\alpha}_{train} - \mu_0(W_{train})),$$

where $\mu_0(\cdot)$ is the prior mean from (5.6) and $K(\cdot, \cdot)$ is the kernel (4.6). We summarize our strategy in Algorithm 4.1.

Algorithm 4.1 Gray-box GPR $m(\mathbf{y})$ training

Input $W, \bar{\mathbf{y}}$ ▷ Parameter locations, Mean-based parameter location

Output $Y_{eval}, m(\cdot), m_{\max}$ ▷ Evaluated locations, $m(\cdot)$ function, maximal valid value of $m(\cdot)$

- 1: $\alpha \leftarrow GP(\mu_0(\cdot), K(\cdot, \cdot)(\cdot, \cdot))$ ▷ Initiate GP (4.4)
 - 2: $\alpha \leftarrow (\mathbf{0}, g^{-1}(1 \text{ iteration}))$
 - 3: $\tau_{PC} \leftarrow PC(\bar{\mathbf{y}})$ ▷ Initialize mean-based PC and store computation time
 - 4: $\mathbf{y}_{\min} = \arg \min_{\mathbf{y} \in W} \mu_0(\mathbf{y}, 1)$
 - 5: $Y_{eval} \leftarrow \{\mathbf{y}_{\min}\}$ ▷ List containing all evaluated parameter locations
 - 6: $\tau_{\mathbf{y}_{\min}}, m_{\mathbf{y}_{\min}} \leftarrow GMRES(\mathbb{A}(\bar{\mathbf{y}})^{-1} \mathbb{A}(\mathbf{y}_{\min}) = \mathbb{A}(\bar{\mathbf{y}})^{-1} b)$ ▷ Initialize by evaluating for smallest $\|\cdot\|_{\gamma,2}$
 - 7: $\tau_{tot}, m_{tot} \leftarrow \tau_{\mathbf{y}_{\min}}, m_{\mathbf{y}_{\min}}$ ▷ Total GMRES iterations computed and time spend on it
 - 8: $\alpha \leftarrow (\mathbf{y}_{\min} - \bar{\mathbf{y}}, g^{-1}(m_{\mathbf{y}_{\min}}))$ ▷ Add training data to the GP
 - 9: $SP \leftarrow \{\}$ ▷ List for SP results

 - 10: **while** running average(SP) > (1% and 1) **do**
 - 11: $m_{\max} \leftarrow \tau_{PC}/(\tau_{tot}/m_{tot})$ ▷ Update the maximal relevant value of $m(\cdot)$
 - 12: $\mathbf{y}_{train} \leftarrow \arg \max \{f_{acq}(\mathbf{y}_i - \bar{\mathbf{y}}; m_{\max}) : \mathbf{y}_i \in (W \setminus Y_{eval}), \}$ ▷ New train point
 - 13: $Y_{eval} \leftarrow Y_{eval} \cup \{\mathbf{y}_{train}\}$
 - 14: $\tau_{\mathbf{y}_{train}}, m_{\mathbf{y}_{train}} \leftarrow GMRES(\mathbb{A}(\bar{\mathbf{y}})^{-1} \mathbb{A}(\mathbf{y}_{train}) = \mathbb{A}(\bar{\mathbf{y}})^{-1} b)$
 - 15: $\alpha \leftarrow (\mathbf{y}_{train} - \bar{\mathbf{y}}, g^{-1}(m_{\mathbf{y}_{train}}))$ ▷ Add training data to GP
 - 16: $SP \leftarrow SP \cup \{SP(g(\mathbb{E}[\alpha]))\}$ ▷ Compute disagreement ratio
 - 17: $\tau_{tot} \leftarrow \tau_{tot} + \tau_{\mathbf{y}_{min}}$ ▷ Bookkeeping
 - 18: $iter_{tot} \leftarrow m_{tot} + m_{\mathbf{y}_{min}}$
 - 19: **end while**

 - 20: **return** $Y_{eval}, g(\mathbb{E}[\alpha(\cdot)]), \tau_{PC}/(\tau_{tot}/m_{tot})$
-

With this approximation $m(\cdot)$ satisfying Assumption 3.1, we can use Algorithm 3.1 to locate the preconditioner locations for the remaining parameter locations. Since a mean-based preconditioner was placed during the Gray-box GPR training, we pass this information on to the location-allocation procedure. Specifically, we run Algorithm 3.1 with $W = W \setminus \{Y_{eval}\}$, $N_{ratio} = m_{\max}$ to discard the already evaluated preconditioners, and the mean-based preconditioner $pc_{fixed} = \{\bar{\mathbf{y}}\}$.

REMARK 4.3 (Parallel training). *Instead of our sequential training approach, parallel approaches could be explored. See, for example, [32, 61].*

5. Helmholtz problem. We study the Truncated Exterior Dirichlet Problem (TEDP) of the Helmholtz equation in two dimensions, where an incoming wave scatters from an impenetrable scatterer with boundary Γ_{in} . We truncate the unbounded

domain with a circle Γ_{out} of radius r_{out} enclosing the scatterer. We use a Robin boundary condition [60] on the scattered wave to approximate the *Dirichlet-to-Neumann map* [49, Section 2.6.3]. Denoting $D = \{\mathbf{x} \in \mathbb{R}^2 : r_{in}(\theta(\mathbf{x})) < \|\mathbf{x}\| < r_{out}\}$, we thus consider the variational problem: for $\mathbf{y} \in Y$, find $u(\mathbf{y}) \in H^1(D)$ such that

$$(5.1) \quad \begin{aligned} & \int_D A(\mathbf{y}) \nabla u(\mathbf{y}) \cdot \nabla v d\mathbf{x} - k_0^2 \int_D n(\mathbf{y}) u(\mathbf{y}) v d\mathbf{x} - ik_0 \int_{\Gamma_{out}} u(\mathbf{y}) v d\mathbf{x} \\ & = \int_{\Gamma_{out}} \left(\frac{\partial}{\partial \hat{\mathbf{n}}} - ik_0 \right) u_{in} v d\mathbf{x}, \quad \text{for all } v \in H^1(D), \end{aligned}$$

where u_{in} is the incoming wave, $n(\mathbf{y}; \cdot)$ is a heterogeneous, real-valued refractive index of the medium, and $A(\mathbf{y}; \cdot)$ a heterogeneous coefficient, taking values in $\mathbb{R}^{2 \times 2}$. Moreover, we require both $n(\mathbf{y}, \cdot)$ and $A(\mathbf{y}, \cdot)$ to be C^1 in \mathbf{y} to go beyond affine expansions in \mathbf{y} .

Discretization with the finite element method leads to linear systems

$$(5.2) \quad \mathbb{A}(\mathbf{y}) \mathbf{u}(\mathbf{y}) = b.$$

To use a-priori bounds from [34], we assume that problem (5.1) is nontrapping, where we denote $\|\cdot\|_{H_{k_0}(D)}^2 := \|\nabla \cdot\|_{L^2(D)}^2 + k_0^2 \|\cdot\|_{L^2(D)}^2$:

ASSUMPTION 5.1 (Nontrapping). *The quantities D , A , and n are such that, given $f \in L^2(D)$, the solution $u(\mathbf{y})$ of (5.1) exists, is unique, and satisfies*

$$\|u(\mathbf{y})\|_{H_{k_0}^1(D)} \leq C_{bound} \|f\|_{L^2(D)},$$

where C_{bound} is independent of k_0 and $\mathbf{y} \in Y$.

For high k_0 , solving (5.2) becomes challenging with GMRES. To solve (5.2) many times for different parameter values, we follow Section 3 to assign the linear systems to a limited number of preconditioners using the surrogate outlined in Section 4. Therefore, we need a good approximation for the prior mean, which we will construct in the next section, and a measure of dimension importance, which we will discuss in Section 5.2.

5.1. The prior mean. Choosing a prior mean is a delicate task. We could use the estimates in [34] and set

$$(5.3) \quad \mu_0(\mathbf{y}, C) := C_1 \|A(\mathbf{y}; \cdot) - A(\hat{\mathbf{y}}; \cdot)\|_{L_{op}^2(D)} + C_2 \|n(\mathbf{y}; \cdot) - n(\hat{\mathbf{y}}; \cdot)\|_{L^2(D)},$$

where C_1 and C_2 are hyperparameters and $\|\cdot\|_{L_{op}^2(D)}$ is the L^2 -norm of the pointwise spectral 2-norm. However, computing this requires integration over D , which is costly.

To evaluate (5.3) efficiently, we exploit the differentiability of A and n :

$$n(\mathbf{y}, \cdot) = n(\hat{\mathbf{y}}, \cdot) + \nabla_{\mathbf{y}} n(\boldsymbol{\eta}^1, \cdot) \cdot (\mathbf{y} - \hat{\mathbf{y}}),$$

for some $\boldsymbol{\eta}^1 \in Y$ between \mathbf{y} and $\hat{\mathbf{y}}$. Expanding the second term in (5.3), we obtain:

$$\begin{aligned} \|n(\mathbf{y}; \cdot) - n(\hat{\mathbf{y}}; \cdot)\|_{L^2(D)} &= \|\nabla_{\mathbf{y}} n(\boldsymbol{\eta}^1, \cdot) \cdot (\mathbf{y} - \hat{\mathbf{y}})\|_{L^2(D)} \\ &= \left((\mathbf{y} - \hat{\mathbf{y}})^\top \mathbb{B}(\boldsymbol{\eta}^1) (\mathbf{y} - \hat{\mathbf{y}}) \right)^{\frac{1}{2}} = \|\mathbf{y} - \hat{\mathbf{y}}\|_{\mathbb{B}(\boldsymbol{\eta}^1)}, \end{aligned}$$

where $\|\cdot\|_{\mathbb{B}(\boldsymbol{\eta}^1)}$ denotes a *weighted* ℓ^2 -norm with a weight matrix $\mathbb{B}(\boldsymbol{\eta}^1)$, parameterized by $\boldsymbol{\eta}^1$. In this case, $\mathbb{B}(\boldsymbol{\eta}^1)$ is a symmetric matrix with entries

$$(5.4) \quad \mathbb{B}_{ij}(\boldsymbol{\eta}^1) = \int_D \partial^{e_i} n(\boldsymbol{\eta}^1, \cdot) \partial^{e_j} n(\boldsymbol{\eta}^1, \cdot) d\mathbf{x}.$$

Similarly, we obtain $\|A(\mathbf{y}; \cdot) - A(\hat{\mathbf{y}}; \cdot)\|_{L^2_{op}(D)} = \|\mathbf{y} - \hat{\mathbf{y}}\|_{\mathbb{D}(\boldsymbol{\eta}^2)}$, where $\mathbb{D}(\boldsymbol{\eta}^2)$ is a symmetric matrix with entries

$$(5.5) \quad \mathbb{D}_{ij}(\boldsymbol{\eta}^2) = \int_D \|\partial^{e_i} A(\boldsymbol{\eta}^2, \cdot) \partial^{e_j} A(\boldsymbol{\eta}^2, \cdot)\|_{2,2} d\mathbf{x},$$

where $\boldsymbol{\eta}^2 \in Y$ lies between \mathbf{y} and $\hat{\mathbf{y}}$ and $\|\cdot\|_{2,2}$ is the spectral matrix norm.

The matrices $\mathbb{B}(\cdot)$ and $\mathbb{D}(\cdot)$ can often be approximated by constant matrices by exploiting the structure of the parameter dependence. We will discuss this for an affine expansion in Section 5.3, and for a parameterized domain in Section 5.4. However, the results presented in both sections are more widely applicable than these two examples, which merely show the process of applying these methods. We also note that, because of the hyperparameters C_1 and C_2 , it is sufficient to know them up to an (unknown) constant.

We can then combine (5.3) with \mathbb{B} and \mathbb{D} to obtain:

$$(5.6) \quad \mu_0(\mathbf{y}|C) = C_1 \|\mathbf{y} - \hat{\mathbf{y}}\|_{\mathbb{D}} + C_2 \|\mathbf{y} - \hat{\mathbf{y}}\|_{\mathbb{B}},$$

for the prior mean of the gray-box Gaussian process (4.4).

5.2. Anisotropy weights. Next to the prior mean, we need a value for the anisotropy weights γ_j proportional to the importance of dimensions in the parameter space. Therefore, we define them in terms of the matrices \mathbb{B} and \mathbb{D} :

$$\gamma_j := C_1 \sqrt{\mathbb{D}_{jj}} + C_2 \sqrt{\mathbb{B}_{jj}},$$

where C_1 and C_2 are the hyperparameters from equation (5.3). Now, the correlation length l_i of the Matérn kernel in dimension i is given by:

$$l_i = \text{diam}(D) \frac{\max_i \gamma_i}{\gamma_i} \geq \text{diam}(D),$$

where $\text{diam}(D)$ is the diameter of the computational domain.

To validate our methods, we will work through two applications. In the next section, Section 5.3, we will consider an affine dependence on the parameter \mathbf{y} for n and in Section 5.4, we consider a parameterized domain test case, where shape of the central scatterer depends on the parameter \mathbf{y} .

5.3. Affine expansion. We investigate affine dependence on the parameter \mathbf{y} for n , and a constant $A = I_2$. The affine expansion of the refractive index n is given by

$$(5.7) \quad n(\mathbf{y}, \mathbf{x}) := n_0(\mathbf{x}) + \sum_{i=1}^N \psi_i(\mathbf{x}) y_i,$$

with $n(\mathbf{y}, \mathbf{x})$ such that the resulting problem is non-trapping problem for all $\mathbf{y} \in Y$ and $\{\psi_i\}$ is uniformly positive over \mathbf{x} .

To apply the methods we developed in Section 4, we need to estimate the matrices \mathbb{D} and \mathbb{B} . Since A is independent of \mathbf{y} , we set $\mathbb{D}_{ij} = 0$. To estimate \mathbb{B} , we use equation (5.4) and compute

$$(5.8) \quad \mathbb{B}_{ij} = \int_D \psi_i(\mathbf{x})\psi_j(\mathbf{x})d\mathbf{x}.$$

In the numerical experiments, we will consider the expansion

$$(5.9) \quad n(\mathbf{y}, \mathbf{x}) := 1 + \sum_{i=1}^N \mathbb{1}_{\Omega_i}(\mathbf{x})\chi(\mathbf{x})\eta_i \frac{y_i - 1}{2},$$

for a partition $\{\Omega_i\}_{i=1}^N$ of D , weights $\eta_i \in \mathbb{R}$, $\mathbf{y} \in Y = [-1, 1]^N$, and χ a mollifier satisfying the assumption below:

ASSUMPTION 5.2. *The mollifier $\chi(\mathbf{x})$ is continuous on D , $\chi(\mathbf{x}) = 1$ on Γ_{in} and $\chi(\mathbf{x}) = 0$ on an open neighbourhood of Γ_{out} .*

By employing a mollifier, we ensure that $n(\cdot, \mathbf{x}) \equiv 1$ and $\nabla_{\mathbf{x}}n(\mathbf{y}, \mathbf{x}) = 0$ on the outer boundary Γ_{out} , to obey the premise of the Sommerfeld radiation condition. Moreover, we choose the partition $\{\Omega_i\}_{i=1}^N$ of D as

$$\Omega_i = \left\{ \mathbf{x} \in D, \frac{2\pi i}{N} \leq \theta(\mathbf{x}) < \frac{2\pi(i+1)}{N} \right\},$$

such that, together with the term $(y_i - 1)$ in (5.9), the non-trapping Assumption 5.1 is fulfilled [33, Condition 2.6]. Moreover, \mathbb{B} is a diagonal matrix with entries $\mathbb{B}_{ii} = C_\chi \eta_i^2$ where $C_\chi \in \mathbb{R}$ is a constant depending on the mollifier that will be absorbed into the hyperparameters. This reduces the correlation lengths to

$$l_i = \text{diam}(D) \frac{\max_j \eta_j}{\eta_i}.$$

For a generic n , the matrix \mathbb{B} from (5.8) can be computed similarly to the techniques we present in the next section.

5.4. Parameterized domain. Our second test case considers scattering against a star-shaped object $\mathcal{D}_{scat}(\mathbf{y})$, parameterized by $\mathbf{y} \in Y = [-1, 1]^N$. Due to this star-shaped property, we can express $\mathcal{D}_{scat}(\mathbf{y})$ in polar coordinates as the region inside a simple, closed curve $r(\mathbf{y}, \theta)$, $\theta \in [0, 2\pi]$:

$$\mathcal{D}_{scat}(\mathbf{y}) = \{ \mathbf{x} \in \mathbb{R}^2 : |\mathbf{x}| \leq r(\mathbf{y}, \theta(\mathbf{x})) \},$$

where $r(\cdot, \theta) \in C_{per}^{0,1}([0, 2\pi])$ for all $\mathbf{y} \in Y$ and $\theta(\mathbf{x})$ is the angle of \mathbf{x} in polar coordinates. The resulting scattering problem is posed on the domain

$$\mathcal{D}(\mathbf{y}) = \{ \mathbf{x} \in \mathbb{R}^2 : r(\mathbf{y}, \theta(\mathbf{x})) \leq |\mathbf{x}| \leq r_{out} \}.$$

We model the boundary $r(\mathbf{y}, \theta)$ as an affine combination of a nominal radius $r_{in}(\theta) \in C_{per}^{0,1}([0, 2\pi])$ and a set of basis functions $\{\psi_j(\theta)\}_{j=1}^N \subset C_{per}^{0,1}([0, 2\pi])$:

$$(5.10) \quad r(\mathbf{y}, \theta) = r_{in}(\theta) + \sum_{j=1}^N \psi_j(\theta)y_j, \quad \text{for all } \theta \in [0, 2\pi] \text{ and } \mathbf{y} \in Y.$$

Moreover, we require $\{\psi_j\}_{j=1}^N$ to be such that $\min_{\mathbf{y} \in Y} \min_{\theta \in [0, 2\pi)} r(\mathbf{y}, \theta) > 0$ ensuring (5.10) defines a non-intersecting curve for all $\mathbf{y} \in Y$. First, we will consider the formulation on the parameterized domain $\mathcal{D}(\mathbf{y})$, and then we will reconnect it to the model problem (5.1) through a mapping approach.

Similarly to the beginning of Section 5, we use a Robin boundary condition and obtain the variational problem: for all $\mathbf{y} \in Y$, find $u(\mathbf{y}) \in H^1(\mathcal{D}(\mathbf{y}))$ such that:

$$(5.11) \quad \int_{\mathcal{D}(\mathbf{y})} A(\mathbf{y}, \mathbf{x}) \nabla u(\mathbf{y}) \cdot \nabla v d\mathbf{x} - k_0^2 \int_{\mathcal{D}(\mathbf{y})} n(\mathbf{y}, \mathbf{x}) u(\mathbf{y}) v d\mathbf{x} - ik_0 \int_{\Gamma_{out}} u(\mathbf{y}) v d\mathbf{x} \\ = \int_{\Gamma_{out}} \left(\frac{\partial}{\partial \hat{n}} - ik_0 \right) u_{in} v d\mathbf{x}, \quad \text{for all } v \in H^1(\mathcal{D}(\mathbf{y})),$$

where A and n are defined on the hold-all domain $\mathcal{D}_H = \cup_{\mathbf{y} \in Y} \mathcal{D}(\mathbf{y})$ satisfying [33, Assumption 2.4] such that they define a nontrapping problem [33, Theorem 2.5]¹. We take care to distinguish u , the solution on the parameterized domain, from u , which will later be the solution on a fixed domain. Without loss of generality, we take $A(\mathbf{y}, \mathbf{x})$ and $n(\mathbf{y}, \mathbf{x})$ constant and set them to one such that, together with the star-shaped property of $\mathcal{D}_{scat}(\mathbf{y})$, we satisfy Assumption 5.1 [46, Prop. 3.1, Chapter 5] with the constant C_{bound} independent of \mathbf{y} [13].

We use a mapping approach [62, 70], in the spirit of [11, 35, 36], on the reference domain to pull the variational formulation (5.11) back to the reference domain $D = \mathcal{D}(\mathbf{0})$. We perform the pullback using a parameter-dependent diffeomorphism $\Phi(\mathbf{y}) : D \mapsto \mathcal{D}(\mathbf{y})$, which we consider to be affinely dependent on the entries of \mathbf{y} [17]:

$$(5.12) \quad \Phi(\mathbf{y}, \mathbf{x}) = \mathbf{x} + \sum_{j=1}^N \Phi_j(\mathbf{x}) y_j, \quad \mathbf{x} \in D,$$

where $\Phi_j(\cdot) \in W^{1, \infty}(D)$ are the partial transformation maps such that $\Phi_j^{-1}(\mathbf{y}, \cdot)$, $\Phi^{-1}(\mathbf{y}, \cdot) \in W^{1, \infty}(D)$. With this, the Courant-Fisher theorem for singular values [38, Thm. 3.1.2] applied to the Jacobian matrices $D_x \Phi(\mathbf{y})$ and $D_x \Phi^{-1}(\mathbf{y})$ ensures that:

$$\sigma_{min} \leq \sigma_1(\mathbf{y}; \mathbf{x}), \dots, \sigma_d(\mathbf{y}; \mathbf{x}) \leq \sigma_{max}, \quad \text{for a.e. } \mathbf{x} \in \mathcal{D}(\mathbf{y}) \text{ and for all } \mathbf{y} \in Y.$$

Denoting by u the pulled back solution, we have the variational problem: for every $\mathbf{y} \in Y$, find $u(\mathbf{y}) \in H^1(D)$ such that

$$\int_D A(\mathbf{y}, \cdot) \nabla u(\mathbf{y}) \cdot \nabla v d\mathbf{x} - k_0^2 \int_D n(\mathbf{y}, \cdot) u(\mathbf{y}) v d\mathbf{x} - ik_0 \int_{\Gamma_{out}} u(\mathbf{y}) v d\mathbf{x} \\ = \int_{\Gamma_{out}} \left(\frac{\partial}{\partial \hat{n}} - ik_0 \right) u_{in} v d\mathbf{x} + \int_D f v d\mathbf{x}, \quad \text{for all } v \in H^1(D),$$

where the coefficients are $A(\mathbf{y}; \mathbf{x}) = D_x \Phi^{-1}(\mathbf{y}; \mathbf{x}) D_x \Phi^{-\top}(\mathbf{y}; \mathbf{x}) \det(D_x \Phi(\mathbf{y}; \mathbf{x}))$ and $n(\mathbf{y}; \mathbf{x}) = \det(D_x \Phi(\mathbf{y}; \mathbf{x}))$. Hence, we are considering a parameterized Helmholtz equation of type (5.1), which we solve using a finite element approach to get linear systems of the form (5.2).

¹To use this result, we require the boundary excitation to be zero. This is not true for our total field equations, but we can use a bound on the linear combination of the scattered field and the total field such as in [14, Corollary 1.6] to obtain the required results.

Similar to the affine expansion in Section 5.3, we still have to obtain the matrices \mathbb{B} and \mathbb{D} by approximating (5.4) and (5.5). To do this, we will use upper bounds in [35] on the first derivative of A and n with respect to \mathbf{y} .

We treat the \mathbb{B} matrix first, by employing [35, Lemma 4] to obtain:

$$|\partial^{e_i} n(\boldsymbol{\eta}^1, \cdot)| \leq 2(1 + \sigma_{\max})^2 \|\Phi_i\|_{W^{1,\infty}(D)}, \quad i = 1, \dots, N,$$

for all $\boldsymbol{\eta}^1$, where σ_{\max} is the upper bound from the Courant-Fisher Theorem, and Φ_i are the partial transformations from equation (5.12). Hence, we bound:

$$\mathbb{B}_{ij}(\boldsymbol{\eta}^1) = \int_D \partial^{e_i} n(\boldsymbol{\eta}^1, \cdot) \partial^{e_j} n(\boldsymbol{\eta}^1, \cdot) d\mathbf{x} \leq C_{\mathbb{B}} \|\Phi_i\|_{W^{1,\infty}(D)} \|\Phi_j\|_{W^{1,\infty}(D)} =: C_{\mathbb{B}} \mathbb{B}_{ij},$$

where the constant $C_{\mathbb{B}} = |D|4(1 + \sigma_{\max})^4$ will be absorbed into the hyperparameter C_2 . Similarly, we use [35, Theorem 4] to bound (5.5):

$$\mathbb{D}_{ij}(\boldsymbol{\eta}^2) \leq C_{\mathbb{D}} \mathbb{D}_{ij},$$

where $\mathbb{D}_{ij} = \mathbb{B}_{ij} = \|\Phi_i\|_{W^{1,\infty}(D)} \|\Phi_j\|_{W^{1,\infty}(D)}$ and $C_{\mathbb{D}} = \frac{16(1+\sigma_{\max})^2}{\sigma_{\min}^2} \frac{4(1+c_\gamma)^2}{\sigma_{\min}^4 \ln(2)^2}$ is a constant which will be absorbed into the hyperparameter C_1 . Moreover, $c_\gamma = \sum_{k=1}^N \|\Phi_k\|_{W^{1,\infty}(D)}$. In the numerical experiments, we will consider a Fourier expansion for $\{\psi_j\}_{j=1}^N$:

$$\psi_j(\theta) := \begin{cases} \vartheta & \text{for } j = 1, \\ \vartheta \left(\frac{j+2}{2}\right)^{-\alpha} \sin(j\theta/2) & \text{for } j \text{ even}, \\ \vartheta \left(\frac{j+1}{2}\right)^{-\alpha} \cos((j-1)\theta/2) & \text{else,} \end{cases}$$

where $\vartheta > 0$ is a scaling constant determining the magnitude of the shape deformations and α a parameter that describes the decay in Fourier modes, introducing anisotropy into the parameter domain. To make sure that $r(\mathbf{y}, \theta)$ in equation (5.10) defines a non-intersecting curve for all parameter dimensions N , we take

$$\vartheta < \vartheta_{\max}(\alpha) := \frac{\inf_{\theta \in [0, 2\pi)} r_{in}(\theta)}{1 + \sqrt{2}(\zeta(\alpha) - 1)},$$

where $\zeta(\alpha)$ is the Riemann Zeta function evaluated at α . Now, combined with the Fourier expansion, we define the partial transformations $\Phi_j(\mathbf{x})$:

$$\Phi_j(\mathbf{x}) := \chi(\mathbf{x}) \psi_j(\theta(\mathbf{x})),$$

with a mollifier satisfying Assumption 5.2 such that we can compute:

$$(5.13) \quad \|\Phi_j\|_{W^{1,\infty}(D)} \leq \begin{cases} 2\vartheta \|\nabla \chi(\mathbf{x})\|_{L^\infty} & \text{for } j = 1, \\ \left(\frac{j+2}{2}\right)^{-\alpha} \vartheta \left(1 + \|\nabla \chi(\mathbf{x})\|_{L^\infty} + \left(\frac{j}{2}\right)\right) & \text{for even } j, \\ \left(\frac{j+1}{2}\right)^{-\alpha} \vartheta \left(1 + \|\nabla \chi(\mathbf{x})\|_{L^\infty} + \left(\frac{j-1}{2}\right)\right) & \text{else.} \end{cases}$$

Finally, we can use the estimates of \mathbb{B} and \mathbb{D} to compute the correlation lengths:

$$l_i = \text{diam}(D) \frac{\max_j \|\Phi_j\|_{W^{1,\infty}(D)}}{\|\Phi_i\|_{W^{1,\infty}(D)}}.$$

6. Numerical illustrations. To show the efficacy of our method, we consider the two test cases outlined in Section 5. In these, we set $r_{in} \equiv \frac{1}{4}$, $r_{out} = 1$, and $r_{mol} = 0.9 < r_{out}$ to define the mollifier

$$\chi(\mathbf{x}) := \frac{|\mathbf{x}| - r_{mol}}{r_{in} - r_{mol}},$$

satisfying Assumption 5.2. We thus have $\text{diam}(D) = 2$ and $\|\nabla\chi(\mathbf{x})\|_{L^\infty} = \frac{1}{r_{mol} - r_{in}}$. We initialize with a mean-based preconditioner at $\bar{\mathbf{y}} = \mathbf{0} \in \mathbb{R}^N$. To test our routine, we consider $|W| = 1000$ points, uniformly spaced in $Y = [-1, 1]^N$.

We implement our numerical methods in Python 3.10, running in an Ubuntu 24.04 Docker container. To obtain the linear systems, we mesh our computational domain using GMesh [30] with uniform mesh size $h \sim k_0^{-\frac{3}{2}}$ to counteract the pollution effect [4]. We use DOLFINx [2, 5, 57, 58] to construct the linear systems, which we solve with GMRES in PETSc [10] until the default relative error (10^{-5}). Moreover, we construct the required preconditioners using PETSc as well. GMRES iterations and PETSc preconditioner construction have been timed using the `time.process_time()` method of the `time` module in Python. We perform the optimization during the location-allocation using the L-BFGS-B Fortran subroutine. When timing pieces of code, we exclude any overhead caused by the assembly of the linear systems (5.2) because we need to assemble them anyway, independently of the preconditioning strategy. We will first focus on the parameterized shape problem, as these results give more insight into the efficacy of the algorithm. Subsequently, we will use the affine case to discuss the effects of isotropy in the parameter domain and to see a practical example of the concentration effect.

6.1. Algorithm performance for the parameterized domain. We demonstrate the improvements of distributed preconditioning over more traditional approaches like mean-based preconditioning, using parameter dimensions ranging from $N = 2$ to $N = 25$.

For each experiment, we report the time to train the gray-box GPR (t_{train}), the location-allocation time (t_{l-al}), and the execution time (t_{exec}) of solving the preconditioned linear systems, rounded to the nearest second, and averaged over several runs to reduce the variance. Moreover, we list the average number of GMRES iterations in the executed strategy (it_{av}). The total computation time ($t_{tot} = t_{train} + t_{l-al} + t_{exec}$) follows. Additionally, we list the average number of placed preconditioners N_{pc} over the runs.

6.1.1. Fixed shape variations and anisotropy. Table 1 shows various results for the shape problem. In Table 1b, we find the results for a medium value for the shape variation parameter ϑ , and we can clearly see that the dimensionality of the problem has a large effect on the algorithm performance. As expected, the gray-box GPR takes longer to train as the parameter dimension increases. Additionally, t_{l-al} increases rapidly with the parameter dimension and this increase is more pronounced than in the training time. This is because the GPR training accounts for parameter dimension anisotropy via the Gaussian process correlation lengths, while the location-allocation does not. On the other hand, the number of preconditioners placed is relatively stable across parameter dimensions.

Finally, when we compute the total computation times $t_{tot} = t_{train} + t_{l-al} + t_{exec}$, we observe that they range from 8,000 to 14,000 seconds, increasing with the parameter

dimension. In these experiments, a single LU preconditioner takes around $t_{pc} = 75$ seconds, leading to a baseline computation time of $|W| * t_{pc} = 75,000$ seconds when not using a preconditioning strategy, significantly more than the observed range for t_{tot} . Therefore, we have realized a significant reduction of the total computation time. A single mean based preconditioner does not work very well in this case, as the number of GMRES iterations rises sharply as $\|\mathbf{y}\| \rightarrow \infty$, for which we do not compare against it. We note that we only know this rises sharply because we have trained the surrogate $m(\cdot)$, it is not clear a-priori whether this is the case or not. Moreover, we observed values for m_{\max} in Equation (4.7) of around 100 throughout these and other experiments.

6.1.2. Varying ϑ . In Table 1a, the maximal shape variation parameter ϑ is double from the baseline, just large enough that no self-intersecting curves can occur. In contrast, Table 1c shows the case when the maximal shape variation is halved with respect to the baseline, resulting in significantly smaller shape variations. This affects matrix values but preserves the overall structure.

Through these experiments, we observe that increasing ϑ raises training time, while reducing ϑ lowers it. For $\vartheta = \frac{1}{4}\vartheta_{\max}(\alpha = 2)$, we observe the same behavior in the training time with respect to the parameter dimension: larger parameter dimensions require more training time. The effect of the parameter dimension is lower in the case of smaller ϑ , as fewer training points are needed to satisfy the stopping criterion. For $\vartheta = \vartheta_{\max}(\alpha = 2)$, we observe similar behavior for N , as we did for $\vartheta_{\frac{1}{2}}\vartheta_{\max}(\alpha = 2)$ where the training time grows rapidly with the parameter dimension.

The number of preconditioners scales with ϑ as $m(\mathbf{y} - \hat{\mathbf{y}})$ grows faster with $\|\mathbf{y} - \hat{\mathbf{y}}\|$. Since t_{pc} and t_{GMRES} , and therefore, by equation (3.1), N_{ratio} , are independent of ϑ , the ‘radius of influence’ of a preconditioner is reduced, and the preconditioners will need to be packed more densely.

The total computation time is mainly determined by the execution time t_{exec} , which increases for larger ϑ . This is partly due to the different number of preconditioners, and partly due to the slightly larger number of Krylov iterations required due to the larger variations in the resulting matrices.

6.1.3. Increased anisotropy. To study the effects of dimension anisotropy, we modify the decay parameter α in Table 1d. Increasing α has two effects: on one hand it decreases the importance of higher parameter dimensions, see equation (5.13) and on the other hand, $\vartheta_{\max}(\alpha = 3) > \vartheta_{\max}(\alpha = 2)$ which we have put to represent total shape variations of the same magnitude.

Foremost, we observe that the values of t_{train} are larger than the values for $\alpha = 2$ due to the larger value of ϑ . On the other side, we see that the train time does not increase much for larger parameter dimensions, clearly showing the effects of the faster decay in the parameter importance. By contrast, location-allocation cost t_{l-al} still rises sharply since it does not account for anisotropy.

6.1.4. Lower and higher frequency. To change problem conditioning and matrix sizes, we modify the frequency k_0 of the Helmholtz equation, shown in Table 2. We consider two cases: a lower frequency of $k_0 = 30$ and a higher frequency $k_0 = 120$. To compare the numerical performance, we keep the size of W the same at 1000 points. However, we emphasise that, when one is interested in the error in a surrogate or an average using Monte Carlo or sparse grid methods, the number of points should be

N	$\vartheta = \vartheta_{\max}(\alpha = 2)$					$\vartheta = \frac{1}{2}\vartheta_{\max}(\alpha = 2)$				
	t_{train}	t_{l-al}	t_{exec}	N_{pc}	it_{av}	t_{train}	t_{l-al}	t_{exec}	N_{pc}	it_{av}
2	1,005	18	12,042	47	10	341	5	7,666	32	7
5	2,092	107	15,599	59	14	421	42	9,785	41	10
10	2,777	554	16,726	70	15	469	166	10,056	34	11
15	2,954	1,239	17,454	59	17	506	447	10,722	39	11
20	4,516	3,412	17,710	60	18	520	1,146	10,962	46	11
25	6,121	5,706	17,943	68	17	597	1,442	11,106	39	12

(a) (b)

N	$\vartheta = \frac{1}{4}\vartheta_{\max}(\alpha = 2)$					$\vartheta = \frac{1}{2}\vartheta_{\max}(\alpha = 3)$				
	t_{train}	t_{l-al}	t_{exec}	N_{pc}	it_{av}	t_{train}	t_{l-al}	t_{exec}	N_{pc}	it_{av}
2	158	3	6,202	19	6	399	5	7,238	29	7
5	174	19	7,295	20	7	455	28	8,267	30	9
10	185	81	7,723	24	8	523	104	8,670	36	9
15	188	299	8,074	21	8	534	245	9,069	38	9
20	174	310	8,151	31	8	631	280	8,587	36	9
25	204	580	7,889	22	8	636	340	9,004	39	9

(c) (d)

Table 1: Results of running Algorithm 3.1 and 4.1 with the shape problem introduced in Section 5.4 with a wavenumbers of $k_0 = 60$. Times in seconds and averaged over multiple runs.

adjusted with k_0 [37]. Due to computational limits, we run our algorithm once for $k_0 = 120$, without averaging over multiple runs.

We observe a large difference in the overall magnitude of the computation times: a low value of k_0 corresponds to low computation times and vice versa in the high frequency case. In the case $k_0 = 30$, we compare the total computation times with the baseline $|W| * t_{pc} \approx 1000 * 1.5 = 1500$ and conclude that we have improved the computational load, but barely when the parameter dimension is large. In the case $k_0 = 120$, we have $|W| * t_{pc} \approx 1000 * 1000s = 1,000,000s \approx 11.5$ days, and we have improved the computational load by a factor of 10.

In the case $k_0 = 30$, the location-allocation cost does not increase as much as the case $k_0 = 60$ (Table 1b), although the number of preconditioners is roughly the same as the dimension increases. This is in contrast to the case $k_0 = 120$, where t_{l-al} increases significantly. We have seen similar increases before in Table 1, where the increase was caused by the higher number of placed preconditioners. In this case, the values of N_{pc} are similar and the increase is due to additional location-allocation steps. The algorithm runs until no further improvements are found or iteration costs exceed the improvement gained, and higher computation times allow more resources for location-allocation iterations. The lower values of t_{l-al} in the case $k_0 = 30$ can be explained similarly. Finally, the number of preconditioners is higher for $k_0 = 30$, which is because τ_{pc} decreases faster than τ_{Krylov} as the matrix dimension shrinks.

6.2. Algorithm performance for the affine expansion. Table 3 shows results for the case of affine expansion outlined in Section 5.3, with a fully isotropic

N	$k_0 = 30, \alpha = 2$					$k_0 = 120, \alpha = 2$				
	t_{train}	t_{l-al}	t_{exec}	N_{pc}	it_{av}	t_{train}	t_{l-al}	t_{exec}	N_{pc}	it_{av}
2	14	12	836	78	5	8,797	6	42,756	23	10
5	23	33	1,114	58	7	20,431	71	55,280	23	17
10	26	162	1,299	56	8	27,018	386	55,221	19	19
15	41	363	1,242	42	8	18,185	1,096	58,667	23	18
20	53	270	1,153	36	7	32,694	3,372	57,725	24	19
25	47	769	1,381	27	10	26,080	5,086	61,619	29	18

(a)

(b)

Table 2: Test results for the shape expansion with $\alpha = 2$, $\vartheta = 2^{-1}\vartheta_{\max}(\alpha = 2)$ and varying frequencies. Times in seconds and averaged over multiple runs.

N	t_{train}	t_{l-al}	t_{exec}	N_{pc}	it_{av}
2	1,551	3	5,339	12	5
5	1,517	11	7,329	7	9
10	1,756	0	7,167	1	10
15	1,627	0	7,501	1	9
20	1,616	0	7,383	1	9
25	1,756	0	7,168	1	9

Table 3: Tabulated results in seconds for affine expansion with $\eta_i = \frac{1}{4}$

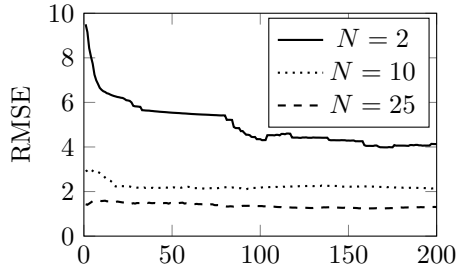


Fig. 2: Training RMSE for affine expansion

parameter domain. This case helps us to study the effects of the parameter anisotropy. We present results with $\eta_i = \frac{1}{4}$, for $i = 1 \cdots N$. This value is not very high, which is reflected in the results.

The most obvious effect is shown in the column N_{pc} , showing only one preconditioner for higher parameter dimensions. This is due to the concentration effect (Remark 3.3) and is in stark contrast to the anisotropic cases discussed before. Thus, we are in fact using mean-based preconditioning, with additional training overhead t_{train} .

Additionally, the training time t_{train} is not significantly impacted by the parameter dimension. This is because the prior mean approximates the surrogate very well, requiring only a few training points. To examine this further, we approximate the root-mean-square error (RMSE) for $N = 2, 10, 25$ during training. Fig. 2 shows that the GPR trains fairly well in the lower dimensional limit, decreasing the RMSE from 10 to 6 quickly, after which the training stagnates. For high dimensions ($N = 25$), the prior fits the model very well, but training does not improve the surrogate. This highlights the curse of dimensionality, showing that parameter anisotropy is necessary for optimal performance.

6.3. Preconditioner placement. We analyze the efficacy of Algorithm 3.1 in placing the preconditioners in Fig. 3. To make this insightful, we use a low parameter dimension of $N = 2$, which allows for clear visualizations, and we sample uniformly over the parameter space. Fig. 3a shows the result of the location-allocation algo-

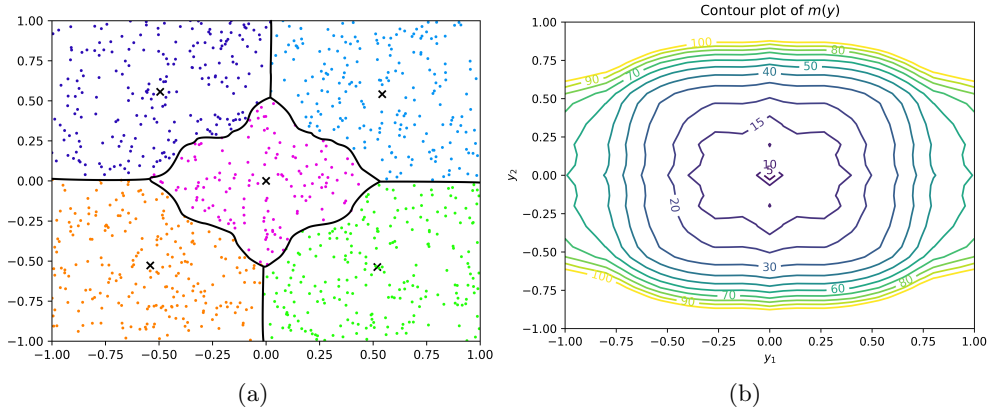


Fig. 3: Result of the location-allocation algorithm; Fig. 3a shows the preconditioner attributions together with the underlying partition of W , and Fig. 3b shows a contour plot of the underlying distance function $m(\cdot)$.

rithm. The colored dots represent the parameter values, and they are grouped by their assigned preconditioner, which is indicated by color. Moreover, in black, the borders of the generalized Voronoi diagram are shown.

From Fig. 3 it is clear that the edges of the Voronoi diagram are curved because the Voronoi distance is based on $m(\cdot)$ shown in Fig. 3b, which deviates from the actual distance to the preconditioner. Moreover, Fig. 3a shows that not all preconditioners are placed at parameter locations, see Remark 3.2.

6.4. Number of preconditioners. Fig. 4 shows the efficacy of the preconditioner count selection in Algorithm 3.1. As discussed in Section 3.3, we re-use the initialization approach for efficiency. To compare against the optimal choice, we perform greedy initialization and execute Algorithm 3.1 after each step. This allows us to check whether our approach is close to the optimal N_{pc} . We perform this comparison for the parameterized shape problem with parameter dimension $N = 15$.

The red line represents the greedy initialization costs, and the blue line corresponds to the costs after the location-allocation are steps taken as long as it is worth the computation time. As expected, there is an optimal number of preconditioners, as the curves exhibit a minimum. The red line being above the blue line indicates that the location-allocation procedure improves preconditioner placement. The black curve shows results if we run location-allocation until full convergence. Since it mostly overlaps with the blue, cutting location-allocation short has little impact, and our strategy is essentially optimal.

Moreover, we observe that the first half of the black and blue curves are a bit volatile, which we would not expect for the global optimum. This volatility occurs because the location-allocation heuristic ends up in local minima, as we discussed back in Section 3.2. Interestingly, other tests that we performed showed that this volatility disappears for both small ($N \leq 5$) and large ($N \geq 25$) values of the parameter dimension. Finally, we see the three curves converging for large values of N_{pc} and indicates that the greedy initialization performs quite well whenever $\frac{|W|}{N_{pc}}$ is small.

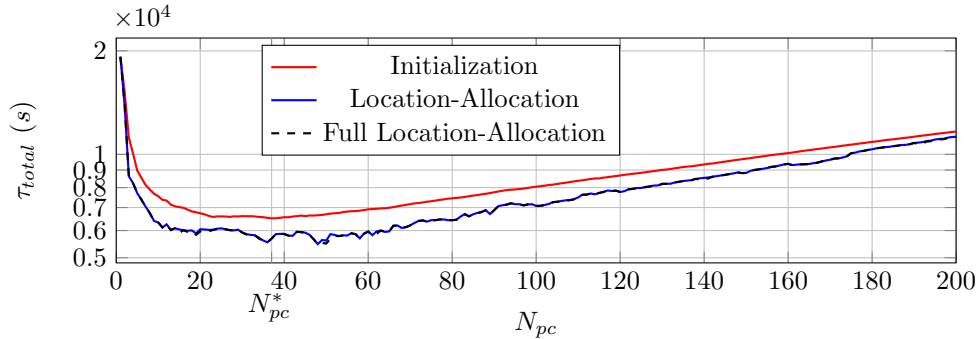


Fig. 4: Effect of different N_{pc} values for the parameterized shape problem. The red curve shows the greedy initialization, the blue curve the location-allocation result from Algorithm 3.1, and the black dashed curve the result of the location-allocation algorithm until convergence. N_{pc}^* is the value where Algorithm 3.1 terminates.

For this run, the chosen value for N_{pc} is at $N_{pc}^* = 35$, marked by a vertical line in Fig. 4. This is lower than the minimum from the greedy initialization, which happened around $N_{pc} \approx 45$. Still, the final strategy remains close to optimal. Variance from local minima overshadows further improvements, making this a cost-effective method.

6.5. Convergence of the surrogate model. The reliability of our preconditioning strategy hinges on a good estimation $m(\cdot)$ for the number of GMRES iterations, which we will explore in this section by using the parameter domain problem with parameter dimension $N = 15$. The results are shown in Fig. 5.

We expect $m(\cdot)$ to predict iterations more accurately with more training data. To verify this, we train the GPR with different numbers of training data N_{train} . After each training point we add, we compute the root-mean-square error of $m(\cdot)$ over the domain $\{\mathbf{y} \in Y | m(\mathbf{y}) < N_{ratio}/2\}$ using a Monte Carlo estimate. This domain is taken such that we measure the accuracy of the surrogate over the relevant domain, as a parameter value with $m(\mathbf{y}) > \frac{N_{ratio}}{2}$ will most likely get assigned to another preconditioner even further from the origin. We use a parameter dimensions $N = 15$, anisotropy $\alpha = 2$, and $\vartheta = \frac{1}{2}\vartheta_{\max}(\alpha = 2)$.

Fig. 5 shows the results: the surrogate accuracy improves with more training data but plateaus at a saturation point. Next to this, we observe that the disagree ratio fluctuates heavily, emphasizing the need for smoothing. Once smoothed, the disagree ratio decays as we add more training data, and it crosses the 1% threshold before the saturation threshold. We observe this behavior consistently across multiple runs and varying parameter dimensions, although the exact stopping point varies. Despite the aggressiveness of the stopping criterion, the surrogate still enables effective preconditioner placement.

Finally, the RMSE converges to a value of approximately 3. This value reflects the modelling error between the actual number of GMRES iterations needed and our surrogate $m(\cdot)$. This originates from our kernel choice, where we assumed a dimensional splitting, together with a symmetry around the origin. These assumptions reduce accuracy but mitigate the curse of dimensionality. A RMSE of 3 is still very acceptable,

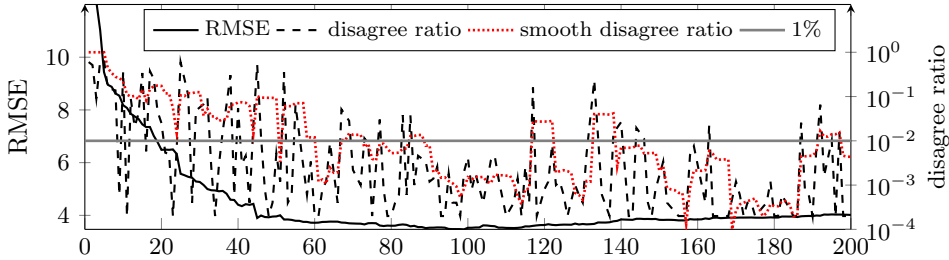


Fig. 5: Comparison of the RMSE and disagree ratio for the stabilizing predictions (SP) stopping criterion. The parameter dimension is $N = 15$ with $\vartheta = \frac{1}{2}\vartheta_{\max}$ and $\alpha = 2$. The solid line represents the RMSE (left axis), the dashed line the disagree ratio, and the dotted line a trailing average of the disagree ratio (right axis). The solid gray line marks the 1% threshold in the stopping criterion.

and the gained computational improvements are well worth it.

7. Discussion and conclusion. In this work, we developed a strategy to place multiple preconditioners in the parameter space that can reduce the computational cost of repeatedly solving parameterized linear systems by an order of magnitude. We use a two-step process: first, we learn a surrogate for the number of Krylov iterations with gray-box Gaussian process regression trained with a cost-aware active learning strategy. This surrogate model allows for estimating optimal number of preconditioners using a greedy approach and finally use a location-allocation algorithm to optimize their locations. We have applied and studied the algorithm thoroughly using a Helmholtz scattering problem.

To choose the *Gaussian process prior*, we use a-priori bounds on the number of GMRES iterations, which are available for the parametric Helmholtz equation [34]. The modeling error caused by the upper bounds is corrected by training the GPR and its hyperparameters. In different applications where such upper bounds are not available, the distance to the origin could be used for the prior mean. Because we use a-priori bounds this way, the prior is more informative and less training is required.

For the *Gaussian process kernel*, we have used a symmetrized Matérn kernel per dimension, summed over all dimensions. This assumption limits the richness of the function space we approximate, and numerical experiments have shown that using a richer full Matérn kernel allows the surrogate to become more accurate, but it suffers more from the curse of dimensionality. Moreover, we notice that, to find large improvements in the total computational burden, a ‘good’ rather than the most accurate surrogate is enough.

For *placing the preconditioners*, we solve a high-dimensional optimization problem where the dimensionality scales with the product of the number of preconditioners and the parameter dimension. We use a location-allocation approach to handle this high dimensionality during preconditioner placement. Since the iterations are costly, we perform them until the improvement is smaller than the computation time. The main cost lies in the location step, where the geometric median of each partition cell W_k has to be computed. Although the cost of this preprocessing step using an off-the-shelf optimizer (L-BFGS-B) is within our requirements, further savings could

be achieved with an ad-hoc optimizer. Unlike previous work [65], we do not require the partitions W_k to be of equal cardinality, possibly resulting in preconditioners with few allocated parameter locations and others with many. However, this is not problematic as we have not considered any multithreaded approaches, which might alter this tradeoff.

Determining the optimal *number of preconditioners* is difficult, as we cannot execute the location-allocation algorithm multiple times, and we thus use a greedy approach. Given the existence of local minima in the preconditioner placement, any further improvements will be overshadowed by these local minima. Since the number and the placement of preconditioners depend on the ratio of preconditioner computation time to Krylov iteration time, our algorithm is the most reliable when there are either no other computational loads or a constant load.

Because of *concentration of measure* effects in high dimensions, our approach will not find significant improvements for high dimensional isotropic parameter spaces. In this case, the optimal number of preconditioners is either one (mean-based preconditioning) or maximal, computing a preconditioner at each parameter location. Adaptive methods can still determine which case is applicable, ensuring that the correct extreme is identified.

Further directions that could be of interest are, among others, the application of different surrogate models, multithreaded approaches, and the use of preconditioners different from the full LU decomposition.

REFERENCES

- [1] C. C. AGGARWAL, A. HINNEBURG, AND D. A. KEIM, *On the Surprising Behavior of Distance Metrics in High Dimensional Space*, in Database Theory – ICDT 2001, Lecture Notes in Computer Science, Springer, 1973, pp. 420–435.
- [2] M. S. ALNÆS, A. LOGG, K. B. ØLGAARD, M. E. ROGNES, AND G. N. WELLS, *Unified form language: A domain-specific language for weak formulations of partial differential equations*, ACM Transactions on Mathematical Software, 40 (2014), pp. 1–37, <https://doi.org/10.1145/2566630>.
- [3] R. ASTUDILLO AND P. I. FRAZIER, *Thinking inside the box: A tutorial on grey-box Bayesian optimization*, in WSC '21: Proceedings of the Winter Simulation Conference, Jan. 2022, <https://doi.org/10.1109/WSC52266.2021.9715343>.
- [4] I. M. BABUŠKA AND S. A. SAUTER, *Is the Pollution Effect of the FEM Avoidable for the Helmholtz Equation Considering High Wave Numbers?*, SIAM Journal on Numerical Analysis, 34 (1997), pp. 2392–2423, <https://doi.org/10.1137/S0036142994269186>.
- [5] I. A. BARATTA, J. P. DEAN, J. S. DOKKEN, M. HABERA, J. S. HALE, C. N. RICHARDSON, M. E. ROGNES, M. W. SCROGGS, N. SIME, AND G. N. WELLS, *DOLFINx: The next generation FEniCS problem solving environment*, Dec. 2023, <https://doi.org/10.5281/ZENODO.10447666>.
- [6] M. BINOIS AND N. WYCOFF, *A Survey on High-dimensional Gaussian Process Modeling with Application to Bayesian Optimization*, ACM Transactions on Evolutionary Learning and Optimization, 2 (2022), pp. 1–26, <https://doi.org/10.1145/3545611>.
- [7] C. M. BISHOP, *Pattern Recognition and Machine Learning*, Information Science and Statistics, Springer, New York, 2006.
- [8] M. BLOODGOOD AND K. VIJAY-SHANKER, *A Method for Stopping Active Learning Based on Stabilizing Predictions and the Need for User-Adjustable Stopping*, in Proceedings of the Thirteenth Conference on Computational Natural Language Learning (CoNLL-2009), Boulder, Colorado, 2009, Association for Computational Linguistics, pp. 39–47.
- [9] J. BRIMBERG, P. HANSEN, N. MLADONOVIC, AND S. SALHI, *A survey of solution methods for the continuous location allocation problem*, International Journal of Operational Research, 5 (2008), pp. 1–12.

- [10] S. B. BROWN, S. ABHYANKAR, M. F. ADAMS, S. BENSON, J. DENER, P. BRUNE, K. BUSCHELMAN, E. M. CONSTANTINESCU, L. DALCIN, AND A. JOLIVET, *PETSc Web page*, 2022.
- [11] J. E. CASTRILLÓN-CANDÁS, F. NOBILE, AND R. F. TEMPONE, *Analytic regularity and collocation approximation for elliptic PDEs with random domain deformations*, *Computers and Mathematics with Applications*, 71 (2016), pp. 1173–1197, <https://doi.org/10.1016/j.camwa.2016.01.005>.
- [12] S. N. CHANDLER-WILDE, I. G. GRAHAM, S. LANGDON, AND E. A. SPENCE, *Numerical-asymptotic boundary integral methods in high-frequency acoustic scattering*, *Acta Numerica*, 21 (2012), pp. 89–305, <https://doi.org/10.1017/S0962492912000037>.
- [13] S. N. CHANDLER-WILDE AND P. MONK, *Wave-Number-Explicit Bounds in Time-Harmonic Scattering*, *SIAM Journal on Mathematical Analysis*, 39 (2008), pp. 1428–1455, <https://doi.org/10.1137/060662575>.
- [14] T. CHAUMONT-FRELET, A. MOIOLA, AND E. A. SPENCE, *Explicit bounds for the high-frequency time-harmonic Maxwell equations in heterogeneous media*, *Journal de Mathématiques Pures et Appliquées*, 179 (2023), pp. 183–218, <https://doi.org/10.1016/j.matpur.2023.09.004>.
- [15] L. P. CHEW AND R. L. S. DYRSDALE, *Voronoi diagrams based on convex distance functions*, in *Proceedings of the First Annual Symposium on Computational Geometry - SCG '85*, Baltimore, Maryland, United States, 1985, ACM Press, pp. 235–244, <https://doi.org/10.1145/323233.323264>.
- [16] R. L. CHURCH, Z. DREZNER, AND A. TAMIR, *Extensions to the Weber problem*, *Computers & Operations Research*, 143 (2022), p. 105786, <https://doi.org/10.1016/j.cor.2022.105786>.
- [17] A. COHEN, C. SCHWAB, AND J. ZECH, *Shape Holomorphy of the Stationary Navier–Stokes Equations*, *SIAM Journal on Mathematical Analysis*, 50 (2018), pp. 1720–1752, <https://doi.org/10.1137/16M1099406>.
- [18] J. COHEN, *A Coefficient of Agreement for Nominal Scales*, *Educational and Psychological Measurement*, 20 (1960), pp. 37–46, <https://doi.org/10.1177/001316446002000104>.
- [19] A. A. CONTRERAS, P. MYCEK, O. P. LE MAÎTRE, F. RIZZI, B. DEBUSSCHERE, AND O. M. KNIO, *Parallel Domain Decomposition Strategies for Stochastic Elliptic Equations Part B: Accelerated Monte Carlo Sampling with Local PC Expansions*, *SIAM Journal on Scientific Computing*, 40 (2018), pp. C547–C580, <https://doi.org/10.1137/17M1132197>.
- [20] L. COOPER, *Location-Allocation Problems*, *Operations Research*, 11 (1963), pp. 331–343, <https://doi.org/10.1287/opre.11.3.331>.
- [21] L. COOPER AND I. KATZ, *The Weber problem revisited*, *Computers & Mathematics with Applications*, 7 (1981), pp. 225–234, [https://doi.org/10.1016/0898-1221\(81\)90082-1](https://doi.org/10.1016/0898-1221(81)90082-1).
- [22] Z. DREZNER, *On the convergence of the generalized Weiszfeld algorithm*, *Annals of Operations Research*, 167 (2009), pp. 327–336, <https://doi.org/10.1007/s10479-008-0336-z>.
- [23] D. DUVENAUD, *Automatic Model Construction with Gaussian Processes*, PhD thesis, Apollo - University of Cambridge Repository, Nov. 2014, <https://doi.org/10.17863/CAM.14087>.
- [24] D. DUVENAUD, H. NICKISCH, AND C. E. RASMUSSEN, *Additive Gaussian Processes*, in *Advances in Neural Information Processing Systems*, vol. 24, Curran Associates, Inc., 2011.
- [25] U. ECKHARDT, *Weber’s problem and weiszfeld’s algorithm in general spaces*, *Mathematical Programming*, 18 (1980), pp. 186–196, <https://doi.org/10.1007/BF01588313>.
- [26] M. EIERMANN, O. G. ERNST, AND E. ULLMANN, *Computational aspects of the stochastic finite element method*, *Computing and Visualization in Science*, 10 (2007), pp. 3–15, <https://doi.org/10.1007/s00791-006-0047-4>.
- [27] H. C. ELMAN, *Iterative Methods for Large, Sparse, Nonsymmetric Systems of Linear Equations*, PhD thesis, Apr. 1982.
- [28] M. EMBREE, *How descriptive are GMRES convergence bounds?*, NA Report 99, 8 (1999).
- [29] O. ERNST, C. E. POWELL, D. SILVESTER, AND E. ULLMANN, *Efficient Solvers for a Linear Stochastic Galerkin Mixed Formulation of Diffusion Problems with Random Data*, *SIAM Journal on Scientific Computing*, 31 (2009), pp. 1424–1447, <https://doi.org/10.1137/070705817>.
- [30] C. GEUZAINÉ AND J.-F. REMACLE, *Gmsh: A 3-D finite element mesh generator with built-in pre- and post-processing facilities*, *International Journal for Numerical Methods in Engineering*, 79 (2009), pp. 1309–1331, <https://doi.org/10.1002/nme.2579>.
- [31] R. G. GHANEM AND R. M. KRUGER, *Numerical solution of spectral stochastic finite element systems*, *Computer Methods in Applied Mechanics and Engineering*, 129 (1996), pp. 289–303, [https://doi.org/10.1016/0045-7825\(95\)00909-4](https://doi.org/10.1016/0045-7825(95)00909-4).
- [32] D. GINSBOURGER, R. LE RICHE, AND L. CARRARO, *Kriging Is Well-Suited to Parallelize Optimization*, in *Computational Intelligence in Expensive Optimization Problems*, L. M. Hiot, Y. S. Ong, Y. Tenne, and C.-K. Goh, eds., vol. 2, Springer Berlin Heidelberg, Berlin, Heidelberg, 2010, pp. 131–162, https://doi.org/10.1007/978-3-642-10701-6_6.

- [33] I. G. GRAHAM, O. R. PEMBERY, AND E. A. SPENCE, *The Helmholtz equation in heterogeneous media: A priori bounds, well-posedness, and resonances*, Journal of Differential Equations, 266 (2019), pp. 2869–2923, <https://doi.org/10.1016/j.jde.2018.08.048>.
- [34] I. G. GRAHAM, O. R. PEMBERY, AND E. A. SPENCE, *Analysis of a Helmholtz preconditioning problem motivated by uncertainty quantification*, Advances in Computational Mathematics, 47 (2021), pp. 1–39, <https://doi.org/10.1007/s10444-021-09889-0>.
- [35] H. HARBRECHT, M. PETERS, AND M. SIEBENMORGEN, *Analysis of the domain mapping method for elliptic diffusion problems on random domains*, Numerische Mathematik, 134 (2016), pp. 823–856, <https://doi.org/10.1007/s00211-016-0791-4>.
- [36] R. HIPTMAIR, L. SCARABOSIO, C. SCHILLINGS, AND C. SCHWAB, *Large deformation shape uncertainty quantification in acoustic scattering*, Advances in Computational Mathematics, 44 (2018), pp. 1475–1518, <https://doi.org/10.1007/s10444-018-9594-8>.
- [37] R. HIPTMAIR, C. SCHWAB, AND E. A. SPENCE, *Frequency-Explicit Shape Holomorphy in Uncertainty Quantification for Acoustic Scattering*, 2024, <https://doi.org/10.48550/ARXIV.2408.01194>.
- [38] R. A. HORN AND C. R. JOHNSON, *Topics in Matrix Analysis*, Cambridge University Press, Apr. 1991, <https://doi.org/10.1017/cbo9780511840371>.
- [39] C. HOWELL, *Lifting the curse of dimensionality: A europeanist’s perspective*, Labor History, 50 (2009), pp. 347–350, <https://doi.org/10.1080/00236560903020930>.
- [40] I. C. F. IPSEN AND C. D. MEYER, *The Idea Behind Krylov Methods*, The American Mathematical Monthly, 105 (1998), pp. 889–899, <https://doi.org/10.1080/00029890.1998.12004985>.
- [41] C. JIN AND X. C. CAI, *A preconditioned recycling GMRES solver for stochastic helmholtz problems*, Communications in Computational Physics, 6 (2009), pp. 342–353, <https://doi.org/10.4208/cicp.2009.v6.p342>.
- [42] D. R. JONES, M. SCHONLAU, AND W. J. WELCH, *Efficient Global Optimization of Expensive Black-Box Functions*, Journal of Global Optimization, 13 (1998), pp. 455–492, <https://doi.org/10.1023/A:1008306431147>.
- [43] P. KALCZYNSKI AND Z. DREZNER, *Further Analysis of the Weber Problem*, Networks and Spatial Economics, (2024), <https://doi.org/10.1007/s11067-024-09627-1>.
- [44] A. KEESE, *Numerical Solution of Systems with Stochastic Uncertainties: A General Purpose Framework for Stochastic Finite Elements*, PhD thesis, Universitätsbibliothek Braunschweig, Apr. 2004, <https://doi.org/10.24355/DBBS.084-200511080100-436>.
- [45] C. L. LARA, F. TRESPALACIOS, AND I. E. GROSSMANN, *Global optimization algorithm for capacitated multi-facility continuous location-allocation problems*, Journal of Global Optimization, 71 (2018), pp. 871–889, <https://doi.org/10.1007/s10898-018-0621-6>.
- [46] P. D. LAX, *Scattering Theory*, no. v. 26 in Pure and Applied Mathematics, Academic Press, Boston, rev. ed ed., 1989.
- [47] P. LUONG, D. NGUYEN, S. GUPTA, S. RANA, AND S. VENKATESH, *Adaptive cost-aware Bayesian optimization*, Knowledge-Based Systems, 232 (2021), p. 107481, <https://doi.org/10.1016/j.knosys.2021.107481>.
- [48] R. M. NEAL, *Monte Carlo Implementation of Gaussian Process Models for Bayesian Regression and Classification*, (1997).
- [49] J.-C. NÉDÉLEC, *Acoustic and Electromagnetic Equations*, vol. 144 of Applied Mathematical Sciences, Springer New York, New York, NY, 2001, <https://doi.org/10.1007/978-1-4757-4393-7>.
- [50] M. L. PARKS, E. DE STURLER, G. MACKEY, D. D. JOHNSON, AND S. MAITI, *Recycling Krylov Subspaces for Sequences of Linear Systems*, SIAM Journal on Scientific Computing, 28 (2006), pp. 1651–1674, <https://doi.org/10.1137/040607277>.
- [51] J. W. PEARSON AND J. PESTANA, *Preconditioners for Krylov subspace methods: An overview*, GAMM Mitteilungen, 43 (2020), pp. 1–35, <https://doi.org/10.1002/gamm.202000015>.
- [52] M. PELLISSETTI AND R. GHANEM, *Iterative solution of systems of linear equations arising in the context of stochastic finite elements*, Advances in Engineering Software, 31 (2000), pp. 607–616, [https://doi.org/10.1016/S0965-9978\(00\)00034-X](https://doi.org/10.1016/S0965-9978(00)00034-X).
- [53] O. R. PEMBERY, *The Helmholtz Equation in Heterogeneous and Random Media: Analysis and Numerics*, PhD thesis, 2020.
- [54] C. E. POWELL AND D. J. SILVESTER, *Preconditioning Steady-State Navier–Stokes Equations with Random Data*, SIAM Journal on Scientific Computing, 34 (2012), pp. A2482–A2506, <https://doi.org/10.1137/120870578>.
- [55] C. E. RASMUSSEN AND C. K. I. WILLIAMS, *Gaussian Processes for Machine Learning*, vol. 7, The MIT Press, 2000.
- [56] P. J. ROUSSEEUW, *Silhouettes: A graphical aid to the interpretation and validation of cluster analysis*, Journal of Computational and Applied Mathematics, 20 (1987), pp. 53–65, [https://doi.org/10.1016/0167-9472\(87\)90023-4](https://doi.org/10.1016/0167-9472(87)90023-4).

- [//doi.org/10.1016/0377-0427\(87\)90125-7](https://doi.org/10.1016/0377-0427(87)90125-7).
- [57] M. W. SCROGGS, I. A. BARATTA, C. N. RICHARDSON, AND G. N. WELLS, *Basix: A runtime finite element basis evaluation library*, Journal of Open Source Software, 7 (2022), pp. 3982–3982, <https://doi.org/10.21105/joss.03982>.
- [58] M. W. SCROGGS, J. S. DOKKEN, C. N. RICHARDSON, AND G. N. WELLS, *Construction of Arbitrary Order Finite Element Degree-of-Freedom Maps on Polygonal and Polyhedral Cell Meshes*, ACM Transactions on Mathematical Software, 48 (2022), pp. 1–23, <https://doi.org/10.1145/3524456>.
- [59] H. D. SHERALI AND F. L. NORDAI, *NP-Hard, Capacitated, Balanced p -Median Problems on a Chain Graph with a Continuum of Link Demands*, Mathematics of Operations Research, 13 (1988), pp. 32–49, <https://doi.org/10.1287/moor.13.1.32>.
- [60] J. J. SHIRRON AND I. BABUŠKA, *A comparison of approximate boundary conditions and infinite element methods for exterior Helmholtz problems*, Computer Methods in Applied Mechanics and Engineering, 164 (1998), pp. 121–139, [https://doi.org/10.1016/S0045-7825\(98\)00050-4](https://doi.org/10.1016/S0045-7825(98)00050-4).
- [61] J. SNOEK, H. LAROCHELLE, AND R. P. ADAMS, *Practical Bayesian Optimization of Machine Learning Algorithms*, in Advances in Neural Information Processing Systems, vol. 25, Curran Associates, Inc., 2012.
- [62] D. M. TARTAKOVSKY AND D. XIU, *Stochastic analysis of transport in tubes with rough walls*, Journal of Computational Physics, 217 (2006), pp. 248–259, <https://doi.org/10.1016/j.jcp.2006.02.029>.
- [63] R. L. THORNDIKE, *Who belongs in the family?*, Psychometrika, 18 (1953), pp. 267–276, <https://doi.org/10.1007/BF02289263>.
- [64] R. TIBSHIRANI, G. WALTHER, AND T. HASTIE, *Estimating the Number of Clusters in a Data Set Via the Gap Statistic*, Journal of the Royal Statistical Society Series B: Statistical Methodology, 63 (2001), pp. 411–423, <https://doi.org/10.1111/1467-9868.00293>.
- [65] N. VENKOVIC, P. MYCEK, O. L. MAÎTRE, AND L. GIRAUD, *Preconditioners based on Voronoi quantizers of random variable coefficients for stochastic elliptic partial differential equations*, 2024, <https://doi.org/10.48550/arXiv.2403.07824>.
- [66] G. WANG AND Q. LIAO, *Efficient Spectral Stochastic Finite Element Methods for Helmholtz Equations with Random Inputs*, East Asian Journal on Applied Mathematics, 9 (2019), pp. 601–621, <https://doi.org/10.4208/eajam.140119.160219>.
- [67] A. J. WATHEN, *Preconditioning*, Acta Numerica, 24 (2015), pp. 329–376, <https://doi.org/10.1017/S0962492915000021>.
- [68] E. WEISZFELD, *Sur le point pour lequel la somme des distances de n points donnees est minimum.*, Tohoku Mathematical Journal, 43 (1937), pp. 355–386.
- [69] Q. XIE, R. ASTUDILLO, P. FRAZIER, Z. SCULLY, AND A. TEREININ, *Cost-aware Bayesian optimization via the Pandora’s Box Gittins index*, arXiv, June 2024, <https://arxiv.org/abs/2406.20062>.
- [70] D. XIU AND D. M. TARTAKOVSKY, *Numerical methods for differential equations in random domains*, SIAM Journal on Scientific Computing, 28 (2006), pp. 1167–1185, <https://doi.org/10.1137/040613160>.